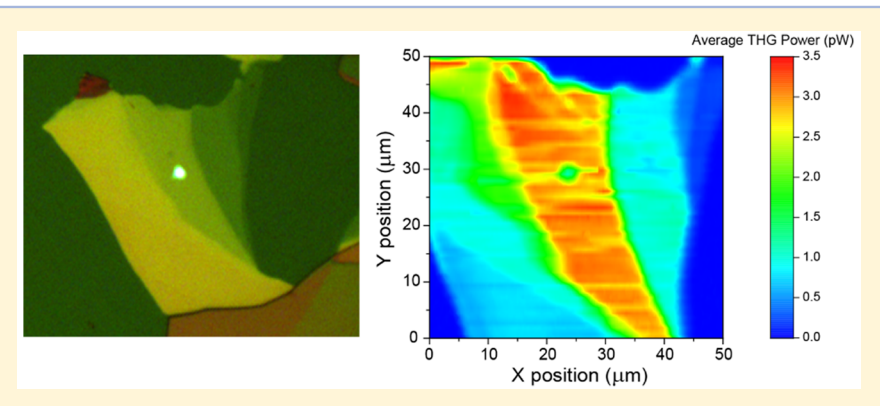


Layer-Tunable Third-Harmonic Generation in Multilayer Black **Phosphorus**

Nathan Youngblood, Ruoming Peng, Andrei Nemilentsau, Tony Low, and Mo Li*

Department of Electrical and Computer Engineering, University of Minnesota, Minnesota, Minnesota 55455, United States

Supporting Information



ABSTRACT: Black phosphorus has been the subject of growing interest due to its unique band structure that is both layer dependent and anisotropic. While many have studied the linear optical response of black phosphorus, the nonlinear response has remained relatively unexplored. Here we report on the observation of third-harmonic generation in black phosphorus using an ultrafast near-IR laser and measure $\chi^{(3)}$ experimentally for the first time. It was found that the third-harmonic emission is highly anisotropic, dependent on the incident polarization, and varies strongly with the number of layers present due to signal depletion and phase-matching conditions.

KEYWORDS: third-harmonic generation, black phosphorus, two-dimensional materials, nonlinear optics

Black phosphorus (BP) recently emerged as a new two-dimensional material with highly unique optical and electrical properties, including high carrier mobility, 1,2 optical and electrical anisotropy,^{3–5} and, importantly, a tunable, direct band gap.^{6–9} Particularly, for thicknesses greater than a few nanometers, BP's band gap bridges the technically important mid-infrared (mid-IR) spectral range that is not currently covered by other two-dimensional semiconductors.⁴ These attributes of BP make it very promising for optoelectronic devices that cover a broad spectral range from near- to mid-IR for both communication and optical sensing. 10,11

In addition to linear optical properties, the quantum confinement in 2D materials also leads to many novel nonlinear optical properties. For example, MoS₂, ¹²⁻¹⁴ WSe₂, ^{15,16} and hBN, 13 all with non-centrosymmetric lattice structures, have shown strong second-order nonlinear optical effects, such as second-harmonic generation (SHG). SHG in these materials has shown strong enhancement at the exciton resonances, 15 can be electrically tuned by a local back gate, 16 and has been utilized for optically probing the crystal orientation ¹² and thickness. ^{13,14}

Additionally, third-order optical nonlinearity such as thirdharmonic generation (THG) has been observed to be strong in graphene, 17,18 as well as in MoS₂ thin films. 19 In terms of nonlinear optics in BP, its centrosymmetric crystalline structure permits only third-order nonlinearity, but its strong anisotropy

and layer-dependent band structure should lead to very intriguing nonlinear optical effects. Research to date, however, has been primarily limited to the saturable absorption effect in BP, studied with z-scan^{20,21} and ultrafast pump-probe²² techniques for liquid exfoliated BP suspensions and utilized for application in mode-locked lasers. ^{23–27} The intrinsic optical nonlinearity of crystalline BP has not been experimentally investigated.

In this paper, we investigate BP's optical nonlinearity by measuring both the polarization and thickness dependence of THG in multilayer BP samples. We find that the THG in BP is strong and highly dependent on both the polarization of the incident light and the number of layers under investigation. From the measurement, BP's third-order nonlinear susceptibility is determined.

RESULTS AND DISCUSSION

Figure 1a shows a typical BP flake used in this paper with the crystal orientation denoted in the lower right-hand side (x- and y-axis indicate the armchair and zigzag directions, respectively). The image shown in Figure 1b shows the THG emission captured by the CCD camera during a measurement. Figure 1c

Received: August 25, 2016 Published: December 12, 2016

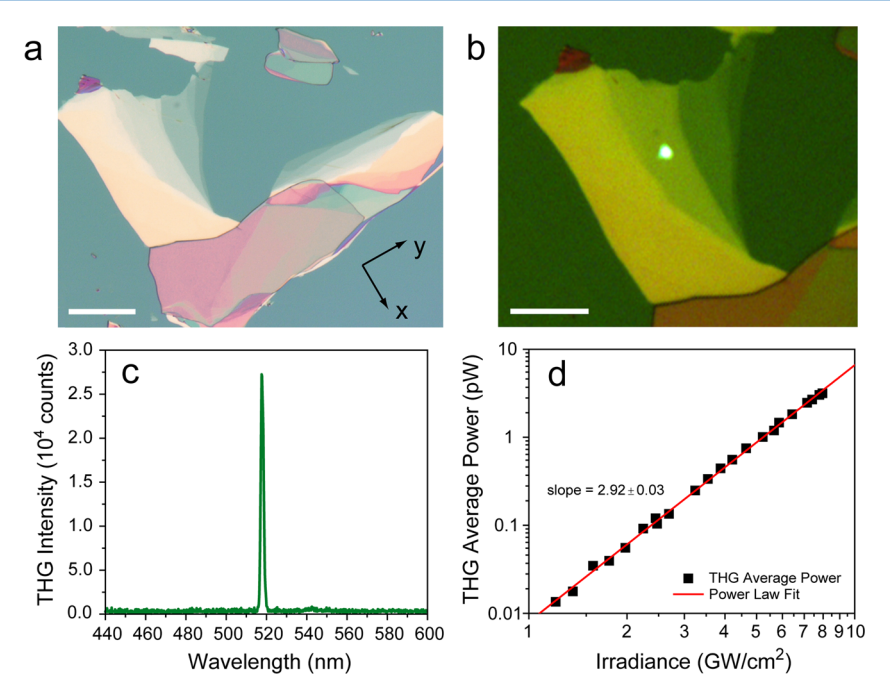


Figure 1. Third-harmonic generation (THG) in multilayer BP. (a) Optical image of black phosphorus flake with multiple layers visible (scale bar 25 μ m). Crystal orientation indicated in lower right. (b) Third-harmonic emission (bright spot) from the flake in (a) measured by a CCD camera (scale bar 20 μ m). (c) Measured spectrum of THG emission with a peak wavelength at 519 nm, which is 3 times the frequency of the fundamental excitation. (d) Power dependence of THG from BP plotted with a power law fit to the data.

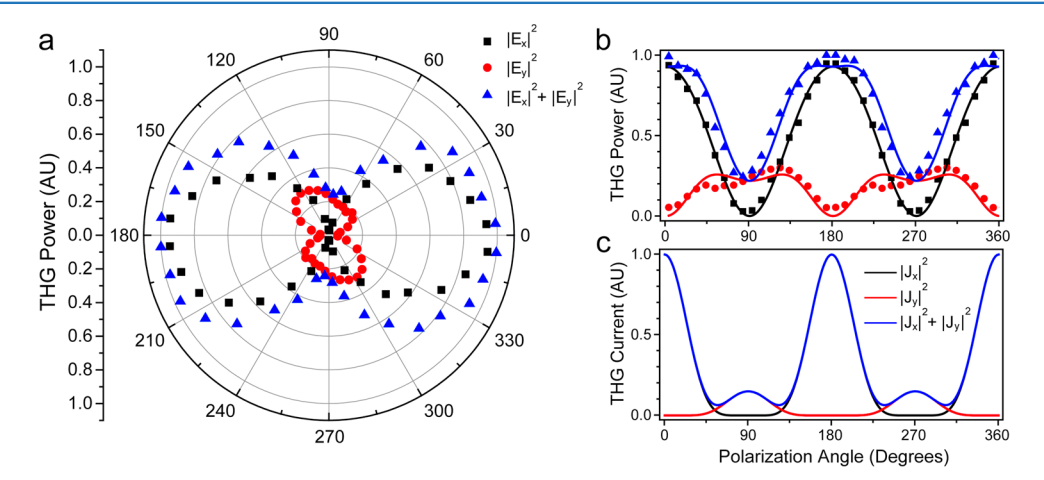


Figure 2. Anisotropic THG in BP. (a) Dependence of THG on the incident polarization. Zero degrees corresponds to the x-axis (armchair direction) of the BP crystal. (b) Same data as in (a) with theoretical fits to the intensity polarized in the x (black squares) and y (red dots) directions. Blue triangles correspond to the total intensity. (c) Calculated THG current induced in BP.

shows a typical spectrum of the third harmonic measured with a visible spectrometer (Ocean Optics USB4000-UV-vis). As expected, the peak response of the THG signal (519 nm) is exactly one-third of the fundamental wavelength of the pump laser (1557 nm). Further confirmation of THG can be seen in Figure 1d, which plots the pump power dependence of the THG power with a power law fit to the experimental data.

Since the linear optical response of BP shows strong anisotropy with the incident light's polarization, 3,28,29 it can be expected that the nonlinear response would show similar anisotropy. The blue triangles in Figure 2a show the angular dependence of the THG emission as a function of incident polarization relative to the α -axis (armchair direction) of the crystal. The minimum in the THG corresponds to an incident polarization aligned along the γ -axis (zigzag direction) of the

crystal. This was verified by photocurrent measurements on other BP flakes with a similar thickness. The polarization angle that minimized the photocurrent (as seen in Yuan et al.³⁰) also minimized the emitted THG power. To extract the polarization dependence of the THG emission, an analyzer was placed in front of the avalanche photodetector (APD) and fixed at either 0 or 90 deg, while a near-IR, half-wave plate was rotated in 5-degree steps to change the linear polarization of the pump laser. The black and red data points in Figure 2a and b correspond to the measured intensity of the α - and α -polarized light, respectively.

BP has an orthorhombic crystal structure and is in the space group *Cmca*.³¹ Knowing this, we can write the contracted third-order nonlinear susceptibility tensor for an orthorhombic crystal exhibiting THG as follows:³²

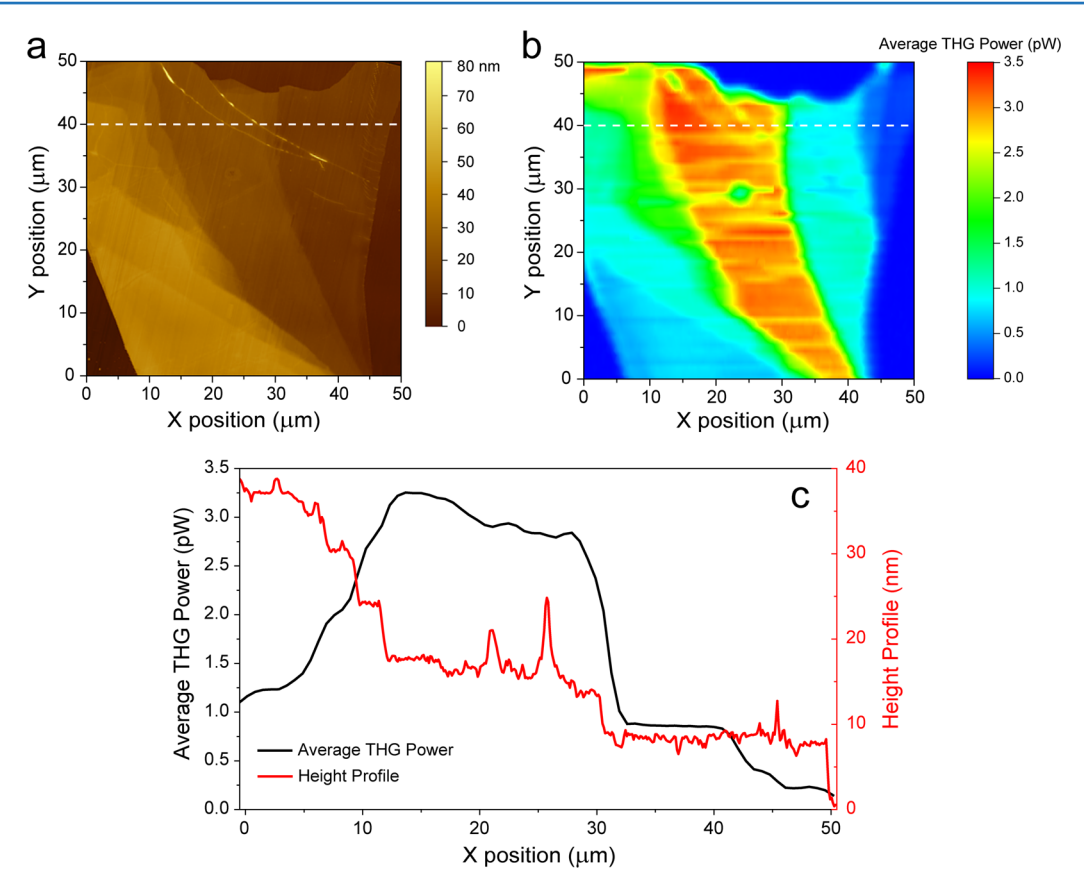


Figure 3. Mapping of the THG signal. (a) Atomic force microscopy (AFM) image of a flake of BP containing many layers of various thicknesses. (b) Position-dependent THG signal measured by scanning the position of the beam relative to the sample. Different thicknesses can be resolved via contrast in the THG signal. (c) Profiles of both the height and THG power extracted from the white cut-lines shown in (a) and (b). THG can show higher contrast than AFM for flake thicknesses less than 15 nm.

$$\begin{bmatrix} \chi_{11} & 0 & 0 & 0 & 0 & \chi_{16} & 0 & \chi_{18} & 0 & 0 \\ 0 & \chi_{22} & 0 & \chi_{24} & 0 & 0 & 0 & 0 & \chi_{29} & 0 \\ 0 & 0 & \chi_{33} & 0 & \chi_{35} & 0 & \chi_{37} & 0 & 0 & 0 \end{bmatrix}$$
(1)

where the first subscript "1, 2, 3" refer to "x, y, z", respectively, and the second subscript signifies the following:

Since we are only exciting in the x-y plane in our configuration, we can set all components that contain a z term to zero. We are left with only four nonzero matrix elements (χ_{11} , χ_{22} , χ_{18} , χ_{29}), which determine the THG in BP. Because the third-harmonic electric field is proportional to the nonlinear susceptibility, we can write the THG output intensity as follows:

$$E_x^2 \propto \left[\chi_{11} \cos^3(\theta) + \chi_{18} \cos(\theta) \sin^2(\theta)\right]^2$$

$$E_y^2 \propto \left[\chi_{22} \sin^3(\theta) + \chi_{29} \sin(\theta) \cos^2(\theta)\right]^2$$
(2)

where θ is the polarization angle relative to the *x*-axis of the crystal. The solid lines in Figure 2b are fits to the measured intensity in the *x* and *y* directions using the relationships in eq 2. One can see good agreement with the overall fit, excluding some asymmetry in the $|E_y|^2$ data. This asymmetry is likely caused by some residual polarization dependence in the

transmission of the dichroic mirror that we were not able to account for during the measurement.

In order to confirm our interpretation, we calculated the density, $j^{(3)}(3\omega)$, of the nonlinear electric current induced in BP at the frequency of third harmonic by the pump field, $E_p =$ $(1/2)E_0^{-i\omega t}$ + c.c. We studied dynamics of the electron subsystem by solving the Liouville equation for a singleelectron density operator, $i\hbar\partial_t \rho = [H, \rho]$, where $H = H_0 + H_{int}$ + $H_{\rm rel}$ is a single-particle Hamiltonian, H_0 is a Hamiltonian of the unperturbed electron system, H_{int} describes the interaction between an electron and the pump, and $H_{\rm rel}$ is the relaxation term (see Supporting Information and Keller et al.³³ and Nemilentsau et al.³⁴ for details). We solved the Liouville equation in the third-order of perturbation theory, $\rho = \sum_{n=0}^{3} \rho^{(3)}$, where $\rho^{(3)} = (1/2)\rho^{(3;3\omega)} e^{-3i\omega t} + (1/2)\rho^{(3;\omega)} e^{-i\omega t} + c.c.$ The term $\rho^{(3;3\omega)}$ describes THG, while $\rho^{(3;\omega)}$ accounts for the self-action effects. The density of the nonlinear current is calculated as $j^{(3)}(3\omega) = \text{Tr}[\rho^{(3;3\omega)}I]$, where I is the current density operator.

In order to keep the calculations tractable, we consider the case of monolayer BP. In this case, the low-energy Hamiltonian is available ²⁹ (see also Supporting Information). The simulation results presented in Figure 2c consider the situation where the pump field is at 0.5 eV, such that the three-photon processes are in resonance with the monolayer gap of 1.5 eV. As one can see, the numerical results are in good qualitative agreement with experimental data. The values of induced current are maximum when the pump field is polarized along the x direction and minimum when polarization is along the y

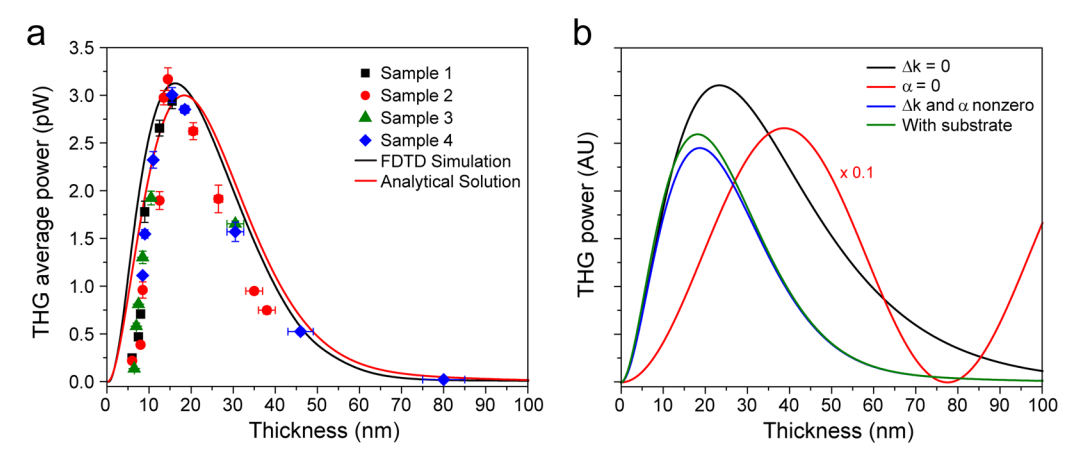


Figure 4. THG dependence on BP thickness. (a) THG average power plotted versus thickness (symbols). Data were extracted from the AFM and THG map of four BP flakes. The solid black line corresponds to full FDTD simulation, where $\chi^{(3)}$ was assumed to be constant and the thickness of the BP layer was varied on a 300 nm SiO₂/Si substrate. The solid red line corresponds to the analytical solution, which includes absorption of the THG signal, which is derived in the Supporting Information. (b) Analytical model of THG in BP showing the contributions of optical absorption, phase mismatch, and reflection of THG from the substrate.

direction. The strong anisotropy is a direct consequence of the band parameters' anisotropy, with the effective mass M_{xx}^* component being considerably smaller than M_{yy}^* . Although the experimental conditions (i.e., frequency and layer numbers) differ from our calculation, we expect similar angular dependence of the induced current at higher frequencies as well, since strong anisotropy of the energy bands imparted by the symmetry of the BP crystalline lattice is also expected far from the band edge. ³⁵

To further characterize the nature of THG in BP, we recorded the power of the THG signal as a function of position by scanning the sample in an x-y grid of 500 nm increments. This allowed us to create a two-dimensional map of the THG power, as can be seen in Figure 3b. We also used atomic force microscopy (AFM) to measure the topography of the various layers present in the same region (Figure 3a). A few wrinkles can be seen in the AFM image that are due to the polydimethylsiloxane (PDMS) transfer process. Interestingly, the two larger wrinkles at the top of the flake can also be seen in the THG map of Figure 3b. Modulation in the optical properties of wrinkled BP has recently been studied where the strain due to wrinkles strongly modifies the band structure and therefore the optical properties of BP. 36

Figure 3c shows the cut-lines for both the topography and THG images denoted by the white lines in Figure 3a and b. One can see that the THG varies significantly as a function of position, but is relatively constant for a fixed flake thickness. Additionally, for thicknesses less than 15 nm, there is much higher contrast between various thicknesses in the THG image compared to the AFM image. We attribute this significant change in the THG power to be largely due to depletion of the THG signal and phase mismatch between the fundamental and THG.

By measuring the average THG power at different positions from Figure 3b and relating it to the height from AFM data in Figure 3a, the THG power as a function of thickness can be extracted. Figure 4a plots the average THG power versus BP thickness from multiple samples. This thickness dependence can be primarily understood by two competing mechanisms. The first is a quadratic increase in the THG signal that is proportional to the square of the number of layers. This assumption is justified for our flakes in the range of 6 to 15 nm

where the thickness is less than the coherence length^{37,38} (backward propagating wave: $L_{\rm coh} = \lambda/6(n_\omega + n_{3\omega}) \approx 40$ nm and forward propagating wave: $L_{\rm coh} = \lambda/6(n_\omega - n_{3\omega}) \approx 870$ nm). As the thickness increases, however, the strong absorption of BP at visible wavelengths contributes to significant depletion of the THG signal as it propagates up through the flake. This can be observed in the exponential decay of the signal at thicknesses greater than 15 nm. Fitting the experimental data with an exponential decay, we estimate the extinction coefficient (the imaginary part of the refractive index) to be κ \approx 2.5. This value is a factor of 2 larger than the value reported by Mao et al. for BP in the visible regime.³⁹ In order to fully account for the depletion of the THG and interference effects of both the fundamental and third-harmonic signal, we performed FDTD simulations using Lumerical Solutions. The excitation source used in the simulation has the same pulse energy and bandwidth as the ultrafast laser used in our experiments. The simulation results are compared with our experimental measurements in Figure 4a, showing a good agreement. However, at small BP thicknesses (<10 nm), the simulation shows the same trend as the experiment, but the absolute values deviate as the flake thickness decreases. One possible explanation is that the exfoliation, transfer, and Al₂O₃ growth negatively affect the first few layers, which accounts for a larger fraction of the total flake for thinner flakes, thus reducing the THG yield. Further studies using fabrication in a more inert environment and van der Waals passivation to preserve the pristine conditions of BP could shed light on this discrepancy.

In order to intuitively understand the general trend in Figure 4a, we plot the thickness-dependent portion of the analytical solution for THG by solving nonlinear Maxwell's equations (see section 2 of the Supporting Information):

$$I_{3\omega}(d) = A(\omega)|\chi^{(3)}|^2 I_{\omega}^{3} \left(\frac{e^{-2\alpha d} - 2\cos(\Delta k d)e^{-\alpha d} + 1}{\alpha^2 + \Delta k^2} \right) e^{-2\alpha d}$$

where d is the thickness of the BP flake, α is the absorption coefficient of the THG signal, and $A(\omega)$ is a scaling factor that includes physical constants and the refractive indices at ω and 3ω . The results of this analytical model can be seen in Figure 4b, where we compare the various effects that optical

absorption, phase mismatch, and reflection from substrate have on the general shape of the curve. We note that although this analytical solution does not consider the absorption and interference of the fundamental pump, simply taking into account the phase mismatch and the absorption of the third-harmonic is enough to describe the general trend we observe in the data. The full FDTD simulations we performed in Figure 4a account for these secondary effects.

It is possible to extract the magnitude of $\chi^{(3)}$ at the peak response (14.5 nm thick) using the result for a thin bulk sample with loss that we derive in the Supporting Information. Taking into account the average power, repetition rate, and spot size of the ultrafast laser (30 mW, 35 MHz, and 5.7 μ m diameter at fwhm) and the refractive index of BP^{29,39} ($n_{\omega} \approx 3.2 + 0.2$ i, $n_{3\omega} \approx 3.5 + 2.5$ i), we estimate the magnitude of $\chi^{(3)}$ to be (1.4 \pm 0.1) \times 10⁻¹⁹ m²/V².

Table 1 compares our results to the experimentally measured values of $\chi^{(3)}$ in other 2D materials reported in the literature.

Table 1. List of $\chi^{(3)}$ Values of Various 2D Materials Reported in the Literature

| number of | | | |
|-----------|---------------------------|--|-----------|
| | (2) (2 = 2) | fundamental | |
| layers | $\chi^{(3)} (m^2/V^2)$ | wavelength (nm) | reference |
| 29 | 1.4×10^{-19} | 1557 | this |
| | | | work |
| 1 | 2.9×10^{-19} | 1560 | 40 |
| >7 | $\sim 10^{-19}$ | 1758 | 19 |
| 1 to 7 | 3.9×10^{-15} | 1560 | 41 |
| 9 to 14 | 1.7×10^{-16} | 1560 | 38 |
| 1 | $\sim 10^{-16}$ | 1720 | 17 |
| 1 | 4×10^{-15} | 1550 | 42 |
| 1 | 1.5×10^{-19} | 1560 | 40 |
| 1 and 2 | $\sim 10^{-19}$ | 789 | 18 |
| | 1 >7 1 to 7 9 to 14 1 1 1 | 29 1.4×10^{-19} 1 2.9×10^{-19} >7 $\sim 10^{-19}$ 1 to 7 3.9×10^{-15} 9 to 14 1.7×10^{-16} 1 $\sim 10^{-16}$ 1 4×10^{-15} 1 1.5×10^{-19} | 29 |

Something directly evident from Table 1 is the wide range of reported results for $\chi^{(3)}$ in graphene. This also influences the estimated $\chi^{(3)}$ for other materials, where the authors directly compare the magnitude of THG in MoS2 and GaSe with a graphene flake on the same substrate and scale $\chi^{(3)}$ accordingly. One explanation is the effect the substrate has on the magnitude of the THG signal observed. 43 Constructive interference of the fundamental pump due to reflections from the substrate can lead to significant enhancements in the power at the graphene layer and lead to overestimates of $\chi^{(3)}$ since the THG signal is proportional to I_1^3 . In our FDTD simulations, we found that using $\chi^{(3)} = 10^{-19} \text{ m}^2/\text{V}^2$ gave a very comparable THG power for the same pulse energy and bandwidth that we used in our experiments, so we believe our estimate of $\chi^{(3)} \approx$ $1.4 \times 10^{-19} \text{ m}^2/\text{V}^2$ from the analytical model to be quite close to the actual value. Another explanation, as pointed out in Woodward et al.,40 is a likely miscalculation in the original estimation of graphene's $\chi^{(3)}$ by Hendry et al., ⁴⁴ which leads to a corrected value of $\chi^{(3)} \approx 10^{-19} \text{ m}^2/\text{V}^2$. Our estimate of $\chi^{(3)}$ is typical for other bulk materials that

Our estimate of $\chi^{(3)}$ is typical for other bulk materials that exhibit a strong third-order optical response³⁷ but an order of magnitude lower than our theoretical prediction of $\chi^{(3)}$ at the band edge (see Supporting Information). It is indeed rather intriguing that the magnitude of $\chi^{(3)}$ in BP is comparable to other 2D materials when the excitation energy used is so far above the band gap of BP. While our initial results are promising, it will be extremely interesting in future works to characterize $\chi^{(3)}$ near the band edge in BP of different

thicknesses, which will require a pump photon energy in the mid-IR regime that is not available in our measurement system.

CONCLUSIONS

In conclusion, we have observed THG in BP thin films using an ultrafast near-IR laser. The third-order response was found to be highly anisotropic with incident polarization. Additionally, we found that the THG was strongly dependent on thickness due to absorption of the third-harmonic signal by BP in addition to interference effects introduced by the substrate. Our study shows that multilayer BP's strong nonlinear and anisotropic optical response could be useful for nonlinear applications. Particularly, at the band edge of BP, that is, for mid-infrared band light, BP's nonlinearity is expected to be very strong and therefore promising for application in mid-infrared nonlinear optics.

Note: During the review process we became aware of another work that studied the third-harmonic response of laser-thinned flakes of BP. 46

METHODS

To prepare our samples, we used Scotch tape to exfoliate single-crystal BP onto glass slides covered with PDMS. Once on the PDMS, suitable BP flakes with multiple layers were identified under an optical microscope and transferred onto silicon substrates coated with 300 nm of thermally grown SiO $_2$. After transferring the BP, the substrates were immediately placed in an atomic layer deposition chamber and coated with 20 nm of $\rm Al_2O_3$ grown at 180 $^{\circ}\rm C$ for passivation to prevent oxidation of the material.

A femtosecond, near-IR fiber laser with a spectrum centered at 1557 nm (photon energy ~0.8 eV) and repetition rate of 35 MHz was used as the pump (200 fs pulse width and 4.4 kW peak power) to probe the THG response of our samples. Light from the laser was focused onto the sample via a near-IR 20× objective (Mitutoyo MPlan NIR, 0.4 NA). A short-pass dichroic filter was used to reflect the fundamental frequency toward the sample, while passing the third harmonic. The filtered light was focused onto either a CCD camera, spectrometer, or APD depending on the measurement.

■ ASSOCIATED CONTENT

S Supporting Information

The Supporting Information is available free of charge on the ACS Publications website at DOI: 10.1021/acsphotonics.6b00639.

Theory of modeling third-harmonic generation; THG-depletion model of THG versus thickness; THG maps and optical images of additional samples used to create Figure 4; third-order autocorrelation measurement (PDF)

AUTHOR INFORMATION

Corresponding Author

*E-mail: moli@umn.edu.

ORCID ®

Nathan Youngblood: 0000-0003-2552-9376

Mo Li: 0000-0002-5500-0900

Notes

The authors declare no competing financial interest.

ACKNOWLEDGMENTS

This work was supported by the Air Force Office of Scientific Research (Award No. FA9550-14-1-0277) and the National Science Foundation (Award No. ECCS-1351002). Device fabrication was carried out at the University of Minnesota Nanofabrication Center, which receives partial support from the NSF through the National Nanotechnology Coordinated Infrastructure (NNCI) program. The authors also used resources at the Characterization Facility, which is a member of the NSF-funded Materials Research Facilities Network via the NSF MRSEC program.

REFERENCES

- (1) Li, L.; Yu, Y.; Ye, G. J.; Ge, Q.; Ou, X.; Wu, H.; Feng, D.; Chen, X. H.; Zhang, Y. Black Phosphorus Field-Effect Transistors. *Nat. Nanotechnol.* **2014**, *9*, 372–377.
- (2) Liu, H.; Neal, A. T.; Zhu, Z.; Luo, Z.; Xu, X.; Tománek, D.; Ye, P. D. Phosphorene: An Unexplored 2D Semiconductor with a High Hole Mobility. *ACS Nano* **2014**, *8*, 4033–4041.
- (3) Qiao, J.; Kong, X.; Hu, Z.-X.; Yang, F.; Ji, W. High-Mobility Transport Anisotropy and Linear Dichroism in Few-Layer Black Phosphorus. *Nat. Commun.* **2014**, *5*, 4475.
- (4) Xia, F.; Wang, H.; Xiao, D.; Dubey, M.; Ramasubramaniam, A. Two-Dimensional Material Nanophotonics. *Nat. Photonics* **2014**, *8*, 899–907
- (5) Wang, X.; Jones, A. M.; Seyler, K. L.; Tran, V.; Jia, Y.; Zhao, H.; Wang, H.; Yang, L.; Xu, X.; Xia, F. Highly Anisotropic and Robust Excitons in Monolayer Black Phosphorus. *Nat. Nanotechnol.* **2015**, *10*, 517–521.
- (6) Takao, Y.; Asahina, H.; Morita, A. Electronic Structure of Black Phosphorus in Tight Binding Approach. *J. Phys. Soc. Jpn.* **1981**, *105*, 3362–3369.
- (7) Tran, V.; Soklaski, R.; Liang, Y.; Yang, L. Layer-Controlled Band Gap and Anisotropic Excitons in Few-Layer Black Phosphorus. *Phys. Rev. B: Condens. Matter Mater. Phys.* **2014**, 89, 235319.
- (8) Kim, J.; Baik, S. S.; Ryu, S. H.; Sohn, Y.; Park, S.; Park, B.-G.; Denlinger, J.; Yi, Y.; Choi, H. J.; Kim, K. S. Observation of Tunable Band Gap and Anisotropic Dirac Semimetal State in Black Phosphorus. *Science* **2015**, 349, 723–726.
- (9) Das, S.; Zhang, W.; Demarteau, M.; Hoffmann, A.; Dubey, M.; Roelofs, A. Tunable Transport Gap in Phosphorene. *Nano Lett.* **2014**, 14, 5733–5739.
- (10) Youngblood, N.; Chen, C.; Koester, S. J.; Li, M. Waveguide-Integrated Black Phosphorus Photodetector with High Responsivity and Low Dark Current. *Nat. Photonics* **2015**, *9*, 249–252.
- (11) Lin, C.; Grassi, R.; Low, T.; Helmy, A. S. Multilayer Black Phosphorus as a Versatile Mid-Infrared Electro-Optic Material. *Nano Lett.* **2016**, *16*, 1683–1689.
- (12) Yin, X.; Ye, Z.; Chenet, D. A.; Ye, Y.; O'Brien, K.; Hone, J. C.; Zhang, X. Edge Nonlinear Optics on a MoS₂ Atomic Monolayer. *Science* **2014**, 344, 488–490.
- (13) Li, Y.; Rao, Y.; Mak, K. F.; You, Y.; Wang, S.; Dean, C. R.; Heinz, T. F. Probing Symmetry Properties of Few-Layer MoS₂ and H-BN by Optical Second-Harmonic Generation. *Nano Lett.* **2013**, *13*, 3329–3333.
- (14) Malard, L. M.; Alencar, T. V.; Barboza, A. P. M.; Mak, K. F.; de Paula, A. M. Observation of Intense Second Harmonic Generation from MoS₂ Atomic Crystals. *Phys. Rev. B: Condens. Matter Mater. Phys.* **2013**, *87*, 201401.
- (15) Wang, G.; Marie, X.; Gerber, I.; Amand, T.; Lagarde, D.; Bouet, L.; Vidal, M.; Balocchi, A.; Urbaszek, B. Giant Enhancement of the Optical Second-Harmonic Emission of WSe₂ Monolayers by Laser Excitation at Exciton Resonances. *Phys. Rev. Lett.* **2015**, *114*, 97403.
- (16) Seyler, K. L.; Schaibley, J. R.; Gong, P.; Rivera, P.; Jones, A. M.; Wu, S.; Yan, J.; Mandrus, D. G.; Yao, W.; Xu, X. Electrical Control of Second-Harmonic Generation in a WSe₂ Monolayer Transistor. *Nat. Nanotechnol.* **2015**, *10*, 407–411.

- (17) Kumar, N.; Kumar, J.; Gerstenkorn, C.; Wang, R.; Chiu, H.-Y.; Smirl, A. L.; Zhao, H. Third Harmonic Generation in Graphene and Few-Layer Graphite Films. *Phys. Rev. B: Condens. Matter Mater. Phys.* **2013**, *87*, 121406.
- (18) Hong, S.-Y.; Dadap, J. I.; Petrone, N.; Yeh, P.-C.; Hone, J.; Osgood, R. M. Optical Third-Harmonic Generation in Graphene. *Phys. Rev. X* **2013**, *3*, 21014.
- (19) Wang, R.; Chien, H.-C.; Kumar, J.; Kumar, N.; Chiu, H.-Y.; Zhao, H. Third-Harmonic Generation in Ultrathin Films of MoS₂. *ACS Appl. Mater. Interfaces* **2014**, *6*, 314–318.
- (20) Lu, S. B.; Miao, L. L.; Guo, Z. N.; Qi, X.; Zhao, C. J.; Zhang, H.; Wen, S. C.; Tang, D. Y.; Fan, D. Y. Broadband Nonlinear Optical Response in Multi-Layer Black Phosphorus: An Emerging Infrared and Mid-Infrared Optical Material. *Opt. Express* **2015**, 23, 11183–11194.
- (21) Zhang, F.; Wu, Z.; Wang, Z.; Wang, D.; Wang, S.; Xu, X. Strong Optical Limiting Behavior Discovered in Black Phosphorus. *RSC Adv.* **2016**, *6*, 20027–20033.
- (22) Wang, Y.; Huang, G.; Mu, H.; Lin, S.; Chen, J.; Xiao, S.; Bao, Q.; He, J. Ultrafast Recovery Time and Broadband Saturable Absorption Properties of Black Phosphorus Suspension. *Appl. Phys. Lett.* **2015**, 107. 91905.
- (23) Sotor, J.; Sobon, G.; Macherzynski, W.; Paletko, P.; Abramski, K. M. Black Phosphorus Saturable Absorber for Ultrashort Pulse Generation. *Appl. Phys. Lett.* **2015**, *107*, 51108.
- (24) Luo, Z.-C.; Liu, M.; Guo, Z.-N.; Jiang, X.-F.; Luo, A.-P.; Zhao, C.-J.; Yu, X.-F.; Xu, W.-C.; Zhang, H. Microfiber-Based Few-Layer Black Phosphorus Saturable Absorber for Ultra-Fast Fiber Laser. *Opt. Express* **2015**, *23*, 20030.
- (25) Mu, H.; Lin, S.; Wang, Z.; Xiao, S.; Li, P.; Chen, Y.; Zhang, H.; Bao, H.; Lau, S. P.; Pan, C.; Fan, D.; Bao, Q. Black Phosphorus-Polymer Composites for Pulsed Lasers. *Adv. Opt. Mater.* **2015**, 3, 1447–1453.
- (26) Chen, Y.; Jiang, G.; Chen, S.; Guo, Z.; Yu, X.; Zhao, C.; Zhang, H.; Bao, Q.; Wen, S.; Tang, D.; Fan, D. Mechanically Exfoliated Black Phosphorus as a New Saturable Absorber for Both Q-Switching and Mode-Locking Laser Operation. *Opt. Express* **2015**, *23*, 12823–12833.
- (27) Lu, D.; Pan, Z.; Zhang, R.; Xu, T.; Yang, R.; Yang, B.; Liu, Z.; Yu, H.; Zhang, H.; Wang, J. Passively Q-Switched Ytterbium-Doped ScBO₃ Laser with Black Phosphorus Saturable Absorber. *Opt. Eng.* **2016**, *55*, 81312.
- (28) Xia, F.; Wang, H.; Jia, Y. Rediscovering Black Phosphorus as an Anisotropic Layered Material for Optoelectronics and Electronics. *Nat. Commun.* **2014**, *5*, 4458.
- (29) Low, T.; Rodin, A. S.; Carvalho, A.; Jiang, Y.; Wang, H.; Xia, F.; Castro Neto, A. H. Tunable Optical Properties of Multilayer Black Phosphorus Thin Films. *Phys. Rev. B: Condens. Matter Mater. Phys.* **2014**, *90*, 75434.
- (30) Yuan, H.; Liu, X.; Afshinmanesh, F.; Li, W.; Xu, G.; Sun, J.; Lian, B.; Curto, A. G.; Ye, G.; Hikita, Y.; Shen, Z.; Zhang, S.-C.; Chen, X.; Brongersma, M.; Hwang, H. Y.; Cui, Y. Polarization-Sensitive Broadband Photodetector Using a Black Phosphorus Vertical P-N Junction. *Nat. Nanotechnol.* **2015**, *10*, 707–713.
- (31) Brown, A.; Rundqvist, S. Refinement of the Crystal Structure of Black Phosphorus. *Acta Crystallogr.* **1965**, *19*, 684–685.
- (32) Yang, X. L.; Xie, S. W. Expression of Third-Order Effective Nonlinear Susceptibility for Third-Harmonic Generation in Crystals. *Appl. Opt.* **1995**, *34*, 6130–6135.
- (33) Keller, O. Random-Phase-Approximation Study of the Response Function Describing Optical Second-Harmonic Generation from a Metal Selvedge. *Phys. Rev. B: Condens. Matter Mater. Phys.* **1986**, 33, 990–1009.
- (34) Nemilentsau, A. M.; Slepyan, G. Y.; Khrutchinskii, A. A.; Maksimenko, S. A. Third-Order Optical Nonlinearity in Single-Wall Carbon Nanotubes. *Carbon* **2006**, *44*, 2246–2253.
- (35) Rudenko, A. N.; Yuan, S.; Katsnelson, M. I. Toward a Realistic Description of Multilayer Black Phosphorus: From G W Approximation to Large-Scale Tight-Binding Simulations. *Phys. Rev. B: Condens. Matter Mater. Phys.* **2015**, 92, 85419.

(36) Quereda, J.; San-Jose, P.; Parente, V.; Vaquero-Garzon, L.; Molina-Mendoza, A. J.; Agraït, N.; Rubio-Bollinger, G.; Guinea, F.; Roldán, R.; Castellanos-Gomez, A. Strong Modulation of Optical Properties in Black Phosphorus through Strain-Engineered Rippling. *Nano Lett.* **2016**, *16*, 2931–2937.

- (37) Boyd, R. W. *Nonlinear Optics*, 3rd ed.; Academic Press: Burlington, MA, 2008.
- (38) Karvonen, L.; Säynätjoki, A.; Mehravar, S.; Rodriguez, R. D.; Hartmann, S.; Zahn, D. R. T.; Honkanen, S.; Norwood, R. A.; Peyghambarian, N.; Kieu, K.; Lipsanen, H.; Riikonen, J. Investigation of Second- and Third-Harmonic Generation in Few-Layer Gallium Selenide by Multiphoton Microscopy. *Sci. Rep.* **2015**, *5*, 10334.
- (39) Mao, N.; Tang, J.; Xie, L.; Wu, J.; Han, B.; Lin, J.; Deng, S.; Ji, W.; Xu, H.; Liu, K.; Tong, L.; Zhang, J. Optical Anisotropy of Black Phosphorus in the Visible Regime. *J. Am. Chem. Soc.* **2016**, *138*, 300–305
- (40) Woodward, R. I.; Murray, R. T.; Phelan, C. F.; de Oliveira, R. E. P.; Runcorn, T. H.; Kelleher, E. J. R.; Li, S.; de Oliveira, E. C.; Fechine, G. J. M.; Eda, G.; de Matos, C. J. S. Characterization of the Secondand Third-Order Nonlinear Optical Susceptibilities of Monolayer MoS₂ Using Multiphoton Microscopy. *arXiv* 2016, 1606.08093.
- (41) Säynätjoki, A.; Karvonen, L.; Rostami, H.; Autere, A.; Mehravar, S.; Lombardo, A.; Norwood, R. A.; Hasan, T.; Peyghambarian, N.; Lipsanen, H.; Kieu, K.; Ferrari, A. C.; Polini, M.; Sun, Z. Ultra-Strong Nonlinear Optical Processes and Trigonal Warping in MoS₂ Layers. arXiv 2016, 1608.04101.
- (42) Säynätjoki, A.; Karvonen, L.; Riikonen, J.; Kim, W.; Mehravar, S.; Norwood, R. A.; Peyghambarian, N.; Lipsanen, H.; Kieu, K. Rapid Large-Area Multiphoton Microscopy for Characterization of Graphene. ACS Nano 2013, 7, 8441–8446.
- (43) Savostianova, N. A.; Mikhailov, S. A. Giant Enhancement of the Third Harmonic in Graphene Integrated in a Layered Structure. *Appl. Phys. Lett.* **2015**, *107*, 18110410.1063/1.4935041
- (44) Hendry, E.; Hale, P. J.; Moger, J.; Savchenko, A. K.; Mikhailov, S. A. Coherent Nonlinear Optical Response of Graphene. *Phys. Rev. Lett.* **2010**, *105*, 10.1103/PhysRevLett.105.097401
- (45) Cheng, J. L.; Vermeulen, N.; Sipe, J. E. Third Order Optical Nonlinearity of Graphene. *New J. Phys.* **2014**, *16*, 05301410.1088/1367-2630/16/5/053014
- (46) Rodrigues, M. J. L. F.; de Matos, C. J. S.; Ho, Y. W.; Peixoto, H.; de Oliveira, R. E. P.; Wu, H.-Y.; Neto, A. H. C.; Viana-Gomes, J. Resonantly Increased Optical Frequency Conversion in Atomically Thin Black Phosphorus. *Adv. Mater.* **2016**, DOI: 10.1002/adma.201603119.